

Published in final edited form as:

Cell Rep. 2014 December 11; 9(5): 1742–1755. doi:10.1016/j.celrep.2014.10.064.

Pharmacogenetic Inhibition of eIF4E-Dependent *Mmp9* mRNA Translation Reverses Fragile X Syndrome-like Phenotypes

Christos G. Gkogkas^{1,8,9,*}, Arkady Khoutorsky^{1,8}, Ruifeng Cao¹, Seyed Mehdi Jafarnejad¹, Masha Prager-Khoutorsky², Nikolaos Giannakas³, Archontia Kaminari³, Apostolia Fragkouli³, Karim Nader⁴, Theodore J. Price⁵, Bruce W. Konicek⁶, Jeremy R. Graff⁶, Athina K. Tzinia³, Jean-Claude Lacaille⁷, and Nahum Sonenberg^{1,*}

¹Department of Biochemistry and Goodman Cancer Research Centre, McGill University, Montréal, QC H3A 1A3, Canada

²Center for Research in Neuroscience, McGill University, Montréal General Hospital, Montréal, QC H3G 1A4, Canada

³Institute of Biosciences and Applications, National Center for Scientific Research Demokritos, Agia Paraskevi, 15310 Athens, Greece

⁴Department of Psychology, McGill University, Montréal, QC H3A 1B1, Canada

⁵School of Behavioral and Brain Sciences, University of Texas at Dallas, Richardson, TX 75080, USA

⁶Lilly Research Laboratories, Eli Lilly and Company, Indianapolis, IN 46285, USA

⁷GRSNC and Department of Neurosciences, Université de Montréal, Montréal, QC H3C 3J7, Canada

SUMMARY

Fragile X syndrome (FXS) is the leading genetic cause of autism. Mutations in *Fmr1* (fragile X mental retardation 1 gene) engender exaggerated translation resulting in dendritic spine dysmorphogenesis, synaptic plasticity alterations, and behavioral deficits in mice, which are reminiscent of FXS phenotypes. Using postmortem brains from FXS patients and *Fmr1* knockout

© 2014 The Authors

This is an open access article under the CC BY-NC-ND license (<http://creativecommons.org/licenses/by-nc-nd/3.0/>).

*Correspondence: christos.gkogkas@ed.ac.uk (C.G.G.), nahum.sonenberg@mcgill.ca (N.S.).

⁸Co-first author

⁹Present address: Patrick Wild Centre and Centre for Integrative Physiology, Hugh Robson Building, University of Edinburgh, Edinburgh EH8 9XD, UK

AUTHOR CONTRIBUTIONS

C.G.G. and N.S. conceived, designed, and supervised the work. C.G.G. and A.K. designed, supervised, and carried out behavioral, electrophysiological, and biochemical experiments. R.C. and M.P.-K. carried out imaging experiments and edited the manuscript. S.M.J. carried out translational profiling experiments. N.G., A.K., A.F., and A.K.T. provided MMP-9 transgenic mice, carried out spine imaging, and designed experiments. K.N. and T.J.P. helped with experimental design. B.W.K. and J.R.G. carried out cercosporamide experiments, edited the manuscript, and helped with experimental design. J.-C.L. supervised electrophysiology experiments and edited the manuscript. C.G.G., A.K., and N.S. wrote the manuscript.

SUPPLEMENTAL INFORMATION

Supplemental Information includes Supplemental Experimental Procedures and six figures and can be found with this article online at <http://dx.doi.org/10.1016/j.celrep.2014.10.064>.

mice (*Fmr1*^{-y}), we show that phosphorylation of the mRNA 5' cap binding protein, eukaryotic initiation factor 4E (eIF4E), is elevated concomitant with increased expression of matrix metalloproteinase 9 (MMP-9) protein. Genetic or pharmacological reduction of eIF4E phosphorylation rescued core behavioral deficits, synaptic plasticity alterations, and dendritic spine morphology defects via reducing exaggerated translation of *Mmp9* mRNA in *Fmr1*^{-y} mice, whereas MMP-9 overexpression produced several FXS-like phenotypes. These results uncover a mechanism of regulation of synaptic function by translational control of *Mmp-9* in FXS, which opens the possibility of new treatment avenues for the diverse neurological and psychiatric aspects of FXS.

INTRODUCTION

Autism spectrum disorders (ASDs) are identified by a cluster of symptoms in three core domains: social interaction, language, and range of interests, but in most cases their etiology is unknown (Elsabbagh et al., 2012). Fragile X syndrome (FXS) is characterized by core deficits in intellectual function, hyperarousal and anxiety, repetitive behaviors, and morphological abnormalities and has a known genetic cause. Many CGG repeats in the *FMR1* gene induce its hypermethylation, transcriptional silencing, and loss of fragile X mental retardation protein (FMRP) expression (Verkerk et al., 1991; Hagerman and Hagerman, 2013). A large percentage of individuals with FXS (~46%) are codiagnosed with ASD (Budimirovic and Kaufmann, 2011). Importantly, FXS is the leading known genetic cause of autism.

FMRP is an RNA-binding protein and binds to several ASD-linked mRNAs (Ascano et al., 2012; Darnell et al., 2011) and represses their translation (Darnell et al., 2011). According to the metabotropic glutamate receptor (mGluR) theory of FXS, loss of FMRP expression in FXS induces exaggerated translation of synaptic plasticity-related mRNAs, downstream of group I mGluR activation (Bear et al., 2004). This mechanism is best demonstrated in *Fmr1*^{-y} mice (*Fmr1* deletion on the X chromosome), which display enhanced rates of translation, aberrant spine morphology (increased numbers of long, thin dendritic spines, which are typical of immature synapses and are also observed in FXS patients) (McKinney et al., 2005; Rudelli et al., 1985), defects in synaptic plasticity (enhanced protein synthesis-dependent mGluR long-term depression [LTD]) (Huber et al., 2001), and morphological/anatomical alterations reminiscent of FXS patients (macroorchidism) (The Dutch-Belgian Fragile X Consortium, 1994; Sutherland and Ashforth, 1979).

The translational inhibitory activity of FMRP is regulated primarily by two intracellular signaling cascades known to couple mGluRs to the translational machinery: the PI3K/Akt/mammalian target of rapamycin (mTOR) (Sharma et al., 2010) and the Ras/ERK (extracellular signal-regulated kinase)/Mnk (mitogen-activated protein kinase interacting kinases) (Osterweil et al., 2010). These pathways stimulate cap-dependent translation by controlling the phosphorylation of translation initiation factors. mTOR phosphorylates 4E-BPs (eukaryotic Initiation Factor 4E-Binding Proteins, which are inhibitors of eIF4E) and S6Ks (ribosomal protein S6 Kinases) to promote translation initiation (Hay and Sonenberg, 2004). Genetic deletion of 4E-BP2 (Gkogkas et al., 2013) or overexpression of eIF4E

(Santini et al., 2013) engenders autism-like behaviors and synaptic plasticity deficits in mice. Genetic removal of S6K1 corrected molecular, synaptic, and behavioral deficits in *Fmr1*^{-/-} mice (Bhattacharya et al., 2012). Moreover, deletion of CPEB1 (cytoplasmic polyadenylation element binding protein 1), an activator of translation, ameliorated biochemical, morphological, electrophysiological, and behavioral phenotypes in *Fmr1*^{-/-} mice (Udagawa et al., 2013).

The Ras/ERK/Mnk pathway stimulates translation largely via phosphorylation of eIF4E on Ser209 by Mnk1 and Mnk2 (Waskiewicz et al., 1997). Phospho-eIF4E has been implicated in the regulation of long-lasting forms of synaptic plasticity and memory (Kelleher et al., 2004). ERK inhibition blocks neuronal activity-induced translation as well as phosphorylation of eIF4E (Kelleher et al., 2004), whereas NMDA receptor activation stimulates the activity of ERK/Mnk and elicits eIF4E phosphorylation (Banko et al., 2004). However, how eIF4E phosphorylation promotes synaptic plasticity and memory and its role in FXS are not known.

Previously, we studied the role of eIF4E phosphorylation in tumorigenesis and prostate cancer progression using a knockin mouse model, where the single phosphorylation site on eIF4E was mutated (Ser209Ala) (Furic et al., 2010). Genome-wide translational profiling in mouse embryonic fibroblasts (MEFs) revealed a subset of mRNAs whose translation was reduced in the *Eif4e*^{ki} (Ser209Ala) mice (Furic et al., 2010). Translation of *Mmp9* mRNA and several additional members of the family of Matrix Metalloproteinases (MMPs) is regulated by eIF4E phosphorylation in MEFs (Furic et al., 2010). Mmp-9 is a gelatinase, which is synthesized as a proprotein, secreted, and activated through cleaving and proteolyzes several components of the extracellular matrix (Huntley, 2012). Mmp-9 plays important roles in spine morphology, synaptic plasticity, and learning and memory (Huntley, 2012).

FMRP inhibits dendritic translation of *Mmp9* mRNA (Janusz et al., 2013); however, the mechanism of this regulation has not been studied. Mmp-9 has been implicated in FXS and ASD. High plasma activity of MMP-9 was reported in individuals with FXS (Dziembowska et al., 2013; Leigh et al., 2013), whereas elevated protein amounts of MMP-9 were detected in amniotic fluid from ASD mothers (Abdallah et al., 2012). Minocycline, a tetracycline derivative, reduced Mmp-9 protein amounts in *Fmr1*^{-/-} mice and improved behavioral and dendritic spine defects (Bilousova et al., 2009; Dansie et al., 2013; Rotschafer et al., 2012). However, minocycline is a broad-spectrum antibiotic targeting several signaling pathways and showing bacteriostatic and immune suppressing activities. Thus, it is imperative to know the causality of MMPs in ASD or FXS and the mechanism leading to increased MMP-9 expression in FXS.

Here, we show that eIF4E phosphorylation is increased in FXS patients' postmortem brains, accompanied by augmented MMP-9 expression, whereas MMP-9 overexpression in mice induces phenotypes reminiscent of FXS. We demonstrate that translation of *Mmp9* mRNA is increased due to elevated eIF4E phosphorylation in *Fmr1*^{-/-} mice. Moreover, genetic reduction of phospho-eIF4E rescues aberrant *Mmp9* mRNA translation and reverses morphological, synaptic, and behavioral deficits in *Fmr1*^{-/-} mice. Pharmacological

inhibition of eIF4E phosphorylation by cercosporamide, a potent inhibitor of Mnk kinases (Konicek et al., 2011), reproduces the morphological, synaptic, and behavioral rescue in *Fmr1*^{-/-} mice. Thus, translational control of *Mmp9* mRNA in response to Mnk-mediated phosphorylation of eIF4E is a mechanism downstream of group 1 mGluRs, which is dysregulated in FXS (Figure S1).

RESULTS

Elevated Phosphorylation of eIF4E and MMP-9 Protein Amounts in FXS Patients and *Fmr1*^{-/-} Mice

To investigate whether eIF4E phosphorylation and MMP-9 expression are altered in FXS, we used postmortem brain samples from FXS patients and age-matched controls. Immunoblot analysis of frontal cortex and hippocampal samples from FXS patients using a phospho-eIF4E (Ser 209) antibody revealed a $37.3\% \pm 2.8\%$ increase in p-eIF4E levels, accompanied by a $42.7\% \pm 3.2\%$ increase in MMP-9 protein amounts, as compared to control individuals (Figures 1A and 1B; Figures S2A and S2B). The increase in p-eIF4E and Mmp-9 protein amounts was recapitulated in *Fmr1*^{-/-} mice (Figures 1C and 1D); p-eIF4E levels were increased by $67.1\% \pm 3.4\%$ and Mmp-9 by $41.1\% \pm 4.1\%$, as compared to wild-type mice (Figures 1C and 1D). Using immunohistochemistry, we observed increased p-eIF4E in the cortex, thalamus, and hippocampus of the *Fmr1*^{-/-} mice (Figures 1E and 1F; Figure S2C). Taken together, these data reveal increased eIF4E phosphorylation and Mmp-9 protein amounts in the brains of FXS patients and *Fmr1*^{-/-} mice.

MMP-9 Overexpression Engenders Autism/FXS-like Phenotypes

Because Mmp-9 is linked to FXS and ASD (Bilousova et al., 2009), we asked whether MMP-9 overexpression would engender FXS-like phenotypes in mice. To this end, we used transgenic (Tg) mice expressing human pro-MMP-9 under the control of the PDGF-B promoter (Fragkouli et al., 2012), mimicking the increase of MMP-9 in FXS patients and *Fmr1*^{-/-} mice (Fragkouli et al., 2012; Figure 1). In *MMP9*-Tg mice, there is an increase in both the latent (pro-) and proteolytically activated forms of MMP-9 (Fragkouli et al., 2012), which is equivalent to the increase observed in *Fmr1*^{-/-} mice (Figures 1C and S2D). To assess whether MMP-9 overexpression causes social behavior deficits, as observed in the *Fmr1*^{-/-} mice, we subjected the *MMP9*-Tg mice to the three-chamber social interaction test (Silverman et al., 2010). Social approach behavior was impaired in *MMP9*-Tg mice, because they failed to show a preference for the social (stranger 1) versus the nonsocial stimulus (empty wire cage; $p > 0.05$, Figure 2A), as compared to wild-type littermates. As expected, *MMP9*-Tg mice were also impaired in the subsequent three-chamber preference for social novelty test (Figure 2A). We then examined the *MMP9*-Tg mice for repetitive/ stereotyped behaviors, which are a hallmark of FXS patients and *Fmr1*^{-/-} mice (Bhattacharya et al., 2012), using the self-grooming test. *MMP9*-Tg mice spent significantly more time ($106.8\% \pm 8.4\%$) grooming than their wild-type littermates, whereas no significant differences were observed in the duration of each grooming bout (Figure 2B).

FXS patients have increased density of immature (filopodial type) dendritic spines (Rudelli et al., 1985). This phenotype is recapitulated in *Fmr1*^{-/-} mice (McKinney et al., 2005).

Using Golgi-Cox staining in *MMP9*-Tg mice, we found increased density of dendritic spines in CA1 hippocampal area ($45.2\% \pm 4.1\%$), along with a decreased number of mature ($54.3\% \pm 2.4\%$; stubby and mushroom type) and increased number of immature ($57.8\% \pm 2.1\%$) spines, as compared to wild-type littermates (Figures 2C–2E). Macroorchidism is commonly diagnosed in FXS patients (Sutherland and Ash-forth, 1979) and is also observed in *Fmr1*^{-/-} mice (Bhattacharya et al., 2012). Testes from *MMP9*-Tg mice at postnatal days 90–100 weighed significantly more ($55.4\% \pm 0.8\%$, Figure 2F), as compared to wild-type littermates. Taken together, these data demonstrate that overexpression of MMP-9 engenders phenotypes similar to those observed in *Fmr1*^{-/-} mice, such as social deficits, repetitive/stereotyped behaviors, and abnormalities in dendritic spine morphology, indicating that increased MMP-9 protein amounts may substantially contribute to FXS pathophysiology.

Exaggerated *Mmp9* mRNA Translation in *Fmr1*^{-/-} Mice Is Alleviated by Genetic Inhibition of eIF4E Phosphorylation

We hypothesized that exaggerated translation in *Fmr1*^{-/-} mice could be rescued by genetically reducing eIF4E phosphorylation, which is a major effector of the hyperactivated Ras/ MAPK/Mnk signaling pathway (Buxade et al., 2008). Importantly, *Mmp9* mRNA is translationally controlled by FMRP at the synapse (Ascano et al., 2012; Darnell et al., 2011; Janusz et al., 2013). We reported that *Mmp9* mRNA is translationally controlled by eIF4E phosphorylation in fibroblasts (Furic et al., 2010). Thus, we sought to investigate whether in the brain the translation of *Mmp9* mRNA is regulated by eIF4E phosphorylation.

We crossed *Fmr1*^{-/-} mice with *Eif4e*^{ki/ki} (knockin; Ser209-Ala) mice (*Eif4e*^{ki}) or with the *Mnk1*^{+/-} /*Mnk2*^{+/-} heterozygote mice (*Mnk*^{het}) to generate “double-mutant” mice (Figure 3A). To assess the effect of the genetic reduction of eIF4E phosphorylation on protein synthesis, we measured de novo protein synthesis in hippocampal slices using puromycin labeling, to tag nascent polypeptide chains (Bhattacharya et al., 2012; Graber et al., 2013; Schmidt et al., 2009). Although we did not detect any significant changes in puromycin incorporation in *Eif4e*^{ki} and *Mnk*^{het} slices (Figure S3A), *Fmr1*^{-/-} hippocampal slices incorporated significantly more puromycin ($55.3\% \pm 6.9\%$), as compared to slices from wild-type mice (Figure 3B), indicating enhanced translation. Puromycin incorporation was significantly reduced in both *Fmr1*^{-/-}/*Eif4e*^{ki} and *Fmr1*^{-/-}/*Mnk*^{het} slices, as compared to *Fmr1*^{-/-} slices, thus demonstrating restoration of protein synthesis, as a result of the reduction in eIF4E phosphorylation (Figures 3B and 3C).

Next, we investigated the effect of reduction of eIF4E phosphorylation in *Fmr1*^{-/-} mice on specific mRNAs. FMRP inhibits the translation of a subset of mRNAs (Ascano et al., 2012; Darnell et al., 2011), either directly through binding to ribosome (Chen et al., 2014) or indirectly by regulating signaling downstream of group 1 mGluRs, impinging upon translation and transcription. We carried out polysome profiling of hippocampal lysates from the four different mouse genotypes examined for global protein synthesis (Figure 3B). No significant changes were detected between the different genotypes in the overall sedimentation profiles of hippocampal tissue (Figure 3D), albeit there was a trend for enhanced association of mRNAs with polysomes in the *Fmr1*^{-/-} mice, when compared to

the other genotypes, as evidenced by the Polysomes/Monosome ratio (Figure S3B). Quantitative RT-PCR (qRT-PCR) analysis of the sucrose density gradient fractions revealed that in accordance with the data in fibroblasts (Furic et al., 2010), *Mmp9* mRNA is associated with lighter polysome fractions in *Eif4e^{ki}* and *Mnk^{het}* mice, as compared to wild-type (WT) mice (Figures S3C and S3D), demonstrating that *Mmp9* mRNA translation is promoted by eIF4E phosphorylation in the brain. Conversely, *Mmp9* mRNA cosediments with heavier polysome fractions in *Fmr1^{-/-}*, as compared to wild-type mice (Figure 3F), indicative of *Mmp9* mRNA enhanced translation in the brain of *Fmr1^{-/-}* mice. It is therefore predicted that in the “double-mutant” strains, *Mmp9* mRNA translation would be restored to wild-type levels, as a result of reduced eIF4E phosphorylation. Indeed, in *Fmr1^{-/-}/Eif4e^{ki}* and *Fmr1^{-/-}/Mnk^{het}* mice, *Mmp9* mRNA distribution is indistinguishable from wild-type mice (Figure 3F). This is also reflected in the amounts of *Mmp9* (Figures 3G and 3H). Importantly, because we did not observe any changes in total *Mmp9* mRNA amounts (Figure 3E) between the different genotypes, increased *Mmp9* protein expression detected in *Fmr1^{-/-}* mice (Figures 1C, 1D, 3G, and 3H) can be explained by increased translation of the *Mmp9* mRNA.

Next, we asked whether translation of other known FMRP target mRNAs, whose expression is enhanced in *Fmr1^{-/-}* mice, is also regulated via eIF4E phosphorylation. We observed reversal of the enhanced translation of mRNAs encoding additional members of the *Mmp* family: *Mmp2*, *Mmp3*, *Mmp7*, and *Mmp24* and of *Dlg4* (PSD-95) mRNAs (Figures S3D and S3E). Notably, decreased eIF4E phosphorylation had no effect on the translation of other known FMRP target mRNAs, such as *Map1b*, *Shank1*, *Shank2*, *Shank3*, *Nr2*, and *Camk2a* (Figures S3D, S3F, and S3G). Taken together, these data demonstrate that genetic reduction of eIF4E phosphorylation negates the exaggerated translation of *Mmp9* mRNA in *Fmr1^{-/-}* mice by attenuating the hyperactivated Ras/MAPK/ Mnk signaling, thus restoring normal rates of translation in *Fmr1^{-/-}* mice.

Genetic Reduction of eIF4E Phosphorylation Reverses Aberrant Dendritic Spine Morphology, Excessive LTD, and FXS-like Behavioral Phenotypes in *Fmr1^{-/-}* Mice

Having determined that MMP-9 overexpression in mice induces phenotypes that are commonly observed in *Fmr1^{-/-}* mice (Figure 2), and that genetic reduction of eIF4E phosphorylation decreases translation of *Mmp9* mRNA in *Fmr1^{-/-}* mice (Figure 3), we investigated whether genetic reduction of eIF4E phosphorylation would rescue abnormalities in dendritic spine morphology, synaptic plasticity, and behavioral deficits in *Fmr1^{-/-}* mice (Figure 4A). Using Golgi-Cox staining in hippocampal CA1 slices from the different mouse genotypes, we observed a decrease in the number of immature and an increase in the number of mature spines in both *Fmr1^{-/-}/Eif4e^{ki}* and *Fmr1^{-/-}/Mnk^{het}* mice, as compared to the *Fmr1^{-/-}* mice (Figures 4B and 4C), which restores the dendritic spine phenotype to wild-type levels. On the other hand, we did not observe any significant changes in CA1 dendritic morphology in *Eif4e^{ki}* or *Mnk^{het}* mice, when compared to wild-type mice (Figure S4A).

Elevated translation in *Fmr1^{-/-}* mice leads to enhanced hippocampal mGluR-LTD (Huber et al., 2001). Consistent with these findings, stimulation of group 1-metabotropic glutamate

receptors led to enhanced mGluR-LTD in *Fmr1*^{-/-} hippocampal slices (Figure 4D). In contrast, mGluR-LTD in hippocampal slices from *Eif4e*^{ki} and *Mnk*^{het} mice was not significantly different from that of wild-type mice (Figure S4B). Input/output curves and paired pulse ratio were also unaffected in *Eif4e*^{ki} and *Mnk*^{het}, as compared to wild-type mice (Figures S5A and S5B). In slices from *Fmr1*^{-/-}/*Eif4e*^{ki} and *Fmr1*^{-/-}/*Mnk*^{het} mice, mGluR-LTD was comparable to that from WT slices and significantly lower than in *Fmr1*^{-/-} slices (Figures 4D and 4E).

Next, we explored the effects of eIF4E phosphorylation on FXS-like behaviors. We first subjected mice to the three-chamber preference for social novelty test. In agreement with previous reports (Bhattacharya et al., 2012), we noted an impaired preference for social novelty in the *Fmr1*^{-/-} mice, whereas WT mice clearly show a preference for the novel social stimulus (stranger 2), as compared to the original social stimulus (stranger 1; Figure 4F). In the “double mutants,” reducing eIF4E phosphorylation rescued the impairment in the preference for social novelty test, as compared to *Fmr1*^{-/-} mice (Figure 4F). To further investigate the reversal of the social behavior impairment, we carried out direct social interaction tests with a juvenile (Figure 4G) or a female mouse (Figure 4H). During the interaction with a juvenile male, *Fmr1*^{-/-} mice displayed aggressive behavior (shorter latency to attack; Figure 4G), but not significant changes in social interaction (time in affiliation; Figure 4G), as compared to wild-type littermates. When an *Fmr1*^{-/-} male interacted with a female mouse, it displayed repetitive behavior, engaging in increased duration of self-grooming, and demonstrated reduced male-female affiliation time (Figure 4H). These data are consistent with previous reports for *Fmr1* knockout in the C57BL/6 background (Bhattacharya et al., 2012). In the “double mutants,” where eIF4E phosphorylation is reduced, there was a complete rescue of the aggressive behavior while interacting with a juvenile mouse (Figure 4G), partial rescue of the repetitive, excessive grooming, and complete rescue of the reduced affiliation while interacting with a female (Figure 4H), as compared to wild-type mice. Yet, in *Eif4e*^{ki} and *Mnk*^{het} mice, there were no significant behavioral changes in the direct social interaction tests with a juvenile male or a female (Figure S4D). Conversely, *Eif4e*^{ki} and *Mnk*^{het} mice display impaired preference for social novelty, as compared to wild-type mice (Figure S4C). This shows that the rescues are specific.

Hyperactivity, seizures, and epilepsy are common symptoms in FXS, which are also exhibited by *Fmr1*^{-/-} mice (Musumeci et al., 2007; Spencer et al., 2005). To assess hyperactivity, we performed the light-dark transition (Figure 4I) and open-field tests (Figure 4J). *Fmr1*^{-/-} mice are significantly more active than wild-type littermates as depicted by the number of light-dark compartment transitions (Figure 4I) and the number of entries and time spent in the center square of the open-field arena (Figure 4J). The “double mutants” showed reversal of hyperactivity/anxiety-like phenotypes in the light-dark and open-field tests (Figures 4I and 4J). We then proceeded to examine the effect of reduced eIF4E phosphorylation on audiogenic seizure susceptibility (AGS), which is age dependent (peak sensitivity at P21). C57BL/6 mice are resistant to AGS (Seyfried et al., 1980). *Fmr1*^{-/-} mice displayed increased tonic-clonic seizures, and respiratory arrest or death (Figure 4K). The “double mutants” were resistant to the induction of AGS, with only a small number of

animals (~25%) displaying AGS. On the other hand, *Eif4e^{ki}* and *Mnk^{het}* mice behavior was comparable to wild-type animals in the light-dark, open-field, and AGS tests (Figure S4E; *Eif4e^{ki}* and *Mnk^{het}* are resistant to AGS, similar to wild-type).

Because MMP-9 overexpression led to a macroorchidism phenotype, we examined whether inhibition of eIF4E phosphorylation (and thus reduced translation of *Mmp9* mRNA) would rescue this FXS-like phenotype. Indeed, “double-mutant” mice display a significant decrease in testicular weight when compared to *Fmr1^{-y}* mice, which constitutes a complete rescue of the macroorchidism phenotype when compared to wild-type mice (Figure S4F). We did not observe any rescue in the novel object recognition or the rotarod (motor coordination) tests (Figures S4G and S4H). However, in these tests, *Fmr1^{-y}* mice displayed significant impairments in accordance with previous reports (Bhattacharya et al., 2012), whereas *Eif4e^{ki}* and *Mnk^{het}* mice performed similarly to wild-type (Figures S4G and S4H). Additionally, we confirmed that the rescue effect was not male specific because also in female *Fmr1^{-/-}* mice genetic reduction of eIF4E phosphorylation corrected impaired preference for social novelty (Figure S2E). In summary, these findings demonstrate that genetic inhibition of eIF4E phosphorylation (which reduces translation of *Mmp9* mRNA) is sufficient to reverse the aberrant dendritic spine morphology, synaptic mGluR-LTD deficits, and several core ASD-like phenotypes in *Fmr1^{-y}* mice.

Chronic Pharmacological Inhibition of eIF4E Phosphorylation Reverses Excessive LTD and FXS-like Phenotypes in *Fmr1^{-y}* Mice

Cercosporamide is a potent inhibitor of Mnk1/Mnk2 kinases (Konicek et al., 2011) (Figure 5A). Cercosporamide has been tested in preclinical models of lung and colon carcinomas, where it substantially reduced proliferation and survival of cancer cells (Konicek et al., 2011). We first studied the effects of cercosporamide on eIF4E phosphorylation in the brain. Following a single intraperitoneal injection of 20 mg/kg of cercosporamide in wild-type mice, we detected a decrease in eIF4E phosphorylation (~25%), whereas a dose of 40 mg/kg led to an ~50% decrease (Figure S5C). Mass spectrometry analysis of brain tissue revealed that cercosporamide was present in the brain, thus demonstrating that it crosses the blood-brain barrier (Figure S5D). To assess the effect of chronic cercosporamide treatment, we injected mice daily for 5 days with various concentrations of cercosporamide and subjected the mice to the three-chamber social interaction test. The 40 mg/kg 5 day regimen impaired social approach behavior in WT mice, whereas the 20 mg/kg had no significant effect (Figure S5E). Importantly, the cercosporamide dose response experiment in *Eif4e^{ki}* and *Mnk^{het}* mice revealed that social approach behavior for both genotypes was not affected by 40 mg/kg for 5 days, indicating that at these concentrations (20–40 mg/kg) the effect of cercosporamide is mediated specifically via eIF4E phosphorylation (Figure S5F). We thus used the 20 mg/kg 5 day treatment as “sub-threshold” and the 40 mg/kg as “above threshold.” Chronic treatment with “subthreshold” cercosporamide concentration reduces eIF4E phosphorylation and expression of *Mmp-9* (Figures 5B and 5C).

Next, we tested whether pharmacological reduction of eIF4E phosphorylation using chronic cercosporamide treatment normalizes elevated general translation in *Fmr1^{-y}* mice. To this end, we prepared hippocampal slices from WT and in *Fmr1^{-y}* mice treated chronically

with 20 mg/kg cercosporamide or vehicle and measured de novo protein synthesis using puromycin labeling. We detected a reversal by cercosporamide of the increase in puromycin incorporation in slices from *Fmr1*^{-/-} mice, but no significant effect in slices from WT mice (Figure S5G).

Having established that cercosporamide crossed the blood-brain barrier and reduced eIF4E phosphorylation, we treated *Fmr1*^{-/-} mice and wild-type littermates with the subthreshold dose of cercosporamide (20 mg/kg, 5 days; Figures 5A–5C). First, we measured dihydroxyphenylglycine (DHPG)-induced mGluR-LTD in CA1 hippocampal slices prepared from vehicle and cercosporamide-treated animals. Cercosporamide-treated *Fmr1*^{-/-} mice displayed a significant decrease in mGluR-LTD (~20%; Figures 5D and 5E), in comparison to vehicle-treated *Fmr1*^{-/-} mice, whereas in wild-type mice the mGluR-LTD was not affected by chronic cercosporamide treatment (Figures 5D and 5E). One injection of cercosporamide (20 mg/kg) had no effect on DHPG-induced mGluR-LTD in *Fmr1*^{-/-} mice (Figures S5H and S5I). Chronic cercosporamide treatment in *Fmr1*^{-/-} mice achieved a complete reversal of several ASD-like behaviors, such as the preference for social novelty impairment (Figure 5F; without affecting social approach behavior in the three-chamber test [Figure S6A]), the aggressive behavior toward a juvenile male (Figure 5G), the reduced sociability and the occurrence of repetitive behaviors (exaggerated self-grooming and reduced affiliation) during the interaction with a female (Figure 5H), the hyperactivity behavior, as illustrated by the increased number of light-dark transitions (Figure 5I) and center-square occupancy in the open-field test (Figure 5J), and finally the increased susceptibility to AGS (Figure 5K). Similarly to the genetic rescue experiments, chronic cercosporamide treatment did not lead to a significant improvement in the rotarod (motor coordination) or novel object recognition tests in *Fmr1*^{-/-} mice (Figures S6B and S6C). It also did not reverse the macro-orchidism phenotype in *Fmr1*^{-/-} mice (Figure S6D). These data constitute a pharmacological approach to selectively reduce eIF4E phosphorylation, and, in conjunction with the genetic rescue (Figure 4), bolster the important role of translational control through eIF4E phosphorylation in rescuing core ASD-like symptoms in *Fmr1*^{-/-} mice.

High-Dose Cercosporamide Impairs Social Approach Behavior in WT but Not *Mmp9*^{-/-} Mice

We showed that translational control through phospho-eIF4E primarily controls a subset of mRNAs (Furic et al., 2010), and in the brain *Mmp* mRNAs are eIF4E key targets (Figures 3 and S3). Taking into account our finding that MMP-9 overexpression in mice induced a subset of phenotypes similar to *Fmr1* knockout mice (Figure 2), we hypothesized that *Mmp*-9, downstream of phospho-eIF4E is a cardinal effector of the Ras/MAPK/Mnk pathway in FXS (Figure 6A). To substantiate this claim, we used *Mmp9*^{-/-} mice injected with 40 mg/kg cercosporamide (5 days). In contrast to *MMP9*-Tg mice, *Mmp9*^{-/-} mice do not display deficits in social interaction, as measured by the three-chamber social interaction test (Figure 6B). The 40 mg/kg cercosporamide dose impairs social approach behavior in WT mice, as evidenced by the significantly reduced interaction of the test mouse with the social stimulus, and the significantly reduced time spent in the social stimulus compartment, in the three-chamber test (Figure 6A). Remarkably, this dose had no significant effect on the

social interaction of *Mmp9*^{-/-} mice (Figure 6B). Taken together, these data show that the effects of cercosporamide are mediated through Mmp9.

Recombinant Active MMP-9, but Not Pro-MMP-9, Abrogates the Rescue of Social Behavior Deficits by Cercosporamide in *Fmr1*^{-/y} Mice

To further establish the role of *Mmp9* in *Fmr1*^{-/y} phenotypes, we used recombinant, active MMP-9, which exhibits a profound stimulatory effect on synaptic potentiation in CA1 (Bozdagi et al., 2007). A single dose (0.1 µg/µl, 2 µl) of active but not inactive pro- *MMP-9* elicits an increase in potentiation in CA1 in vivo (Bozdagi et al., 2007). We postulated that proteolytically active MMP-9 infusion should occlude the rescue effects of chronic cercosporamide treatment in *Fmr1*^{-/y} mice. To this end, we treated *Fmr1*^{-/y} mice with the chronic cercosporamide dose (20 mg/kg) and simultaneously infused through cannulas active or prorecombinant MMP-9 (two doses per day for 5 days, 0.1 µg/µl, 2 µl per dose). The mice were then tested in the preference for social novelty test. Infusion of active MMP-9 but not of the proform was sufficient to block the rescue effects of chronic cercosporamide treatment in *Fmr1*^{-/y} mice, as demonstrated by the impaired preference for social novelty (Figure 6C).

These findings, together with the resistance of *Mmp9*^{-/-} mice to high-dose cercosporamide (Figure 6B), demonstrate that translational control of *Mmp9* mRNA through eIF4E phosphorylation is a regulatory mechanism in *Fmr1*^{-/y} mice, which could be dysregulated in FXS.

DISCUSSION

Here, we showed that FXS patients display an increase in MMP-9 protein and phospho-eIF4E levels in the brain (Figure 1). Overexpression of MMP-9 in mice recapitulates major *Fmr1*^{-/y} phenotypes (Figure 2). We also demonstrate that genetic inhibition of eIF4E phosphorylation reduces *Mmp9* mRNA translation (Figure 3). Likewise, genetic or pharmacological inhibition (cercosporamide) of phospho-eIF4E rescues FXS-like phenotypes in *Fmr1*^{-/y} mice (Figures 4 and 5). Thus, we postulate that a substantial fraction of the FXS-like phenotypes in *Fmr1*^{-/y} mice can be explained by exaggerated phospho-eIF4E-dependent *Mmp9* mRNA translation.

Reversal of Exaggerated Translation in *Fmr1*^{-/y} Mice by Phospho-eIF4E Inhibition

A hallmark of *Fmr1* deletion in mice is an increase in global protein synthesis, due to the absence of the translational “brake” that FMRP sets downstream of group 1 mGluRs (Bhattacharya et al., 2012; Huber et al., 2001; Osterweil et al., 2013; Udagawa et al., 2013). In *Fmr1* knockout mice, mutation of the single phosphorylation site on eIF4E or haploinsufficiency of *Mnk1* and *Mnk2* restored the general translation rates (Figure 3). However, translation was not restored for all FMRP mRNA targets. Restoring translation through normalizing eIF4E phosphorylation primarily affected *Mmps* (*Mmp9*, *Mmp2*, *Mmp3*, *Mmp7*, and *Mmp24*) and *Dlg4* (PSD-95) (Figure S3), but not other FMRP targets such as *Camk2a* (CamKIIa), *Shanks*, or *Map1B*. This is similar to findings in *Fmr1/S6K1* double-knockout mice, inasmuch as restoration of translation following ablation of S6K1

affects translation of most, but not all FMRP target mRNAs (Bhattacharya et al., 2012). Thus, it is likely that, downstream of group 1 mGluRs, different translation pathways such as 4EBPs, S6Ks, and phospho-eIF4E govern the translation of distinct pools of neuronal mRNAs.

Genetic or Pharmacological Inhibition of eIF4E Phosphorylation Restores Core FXS Behaviors in *Fmr1*^{-/-} Mice

Excessive Ras/Erk signaling was reported in FXS patients (Wang et al., 2012). We demonstrated increased phosphorylation of eIF4E, which is a downstream target of the Ras/Erk signaling, along with increased expression of MMP-9 in postmortem brain samples (Figure 1). These findings in conjunction with increased phosphorylation of eIF4E in FXS patients lymphocytes (Hoeffler et al., 2012) and increased MMP-9 protein expression in amniotic fluid of ASD mothers (Abdallah et al., 2012) raise the possibility that phospho-eIF4E regulation may be used to diagnose FXS or ASD at earlier ages. Alanine mutation of the phospho-Ser209 site in eIF4E or deletion of one copy of Mnk1 and Mnk2 causes a reduction in eIF4E phosphorylation (Figures 3 and 4). Similarly, using cercosporamide, a Mnk1/ Mnk2 inhibitor, we were able, following chronic treatment, to reduce eIF4E phosphorylation (Figure 5). In all cases, we achieved a rescue of the exaggerated protein synthesis, the enhanced mGluR-LTD (without affecting input/output and paired pulse ratio [Figures S5A and S5B]), the immature CA1 dendritic spine morphology, and the FXS-like behaviors (preference for social novelty, aspects of social interaction with juvenile males and females, light-dark transition, open-field exploration, and audiogenic seizures; Figures 4 and 5).

Cercosporamide Selectively Inhibits eIF4E Phosphorylation and Reverses FXS-like Phenotypes

Our findings highlight cercosporamide as an inhibitor of eIF4E phosphorylation in the brain (Figure 5; Figures S5 and S6), which reverses a number of FXS-like phenotypes in adult *Fmr1*^{-/-} mice. We showed that (1) a chronic subthreshold 20 mg/kg dose does not affect social behavior in WT, *Mnk^{het}*, or *Eif4e^{ki}* mice and (2) a chronic 40 mg/kg above-threshold dose impairs social interaction in WT mice, but not in *Mnk^{het}* or *Eif4e^{ki}* (Figure S5). These data indicate that our rescue experiments were carried out using a concentration range where cercosporamide does not have any off-target effects. Infusion of the active but not the latent form of recombinant MMP-9 abrogated the rescue effect of chronic cercosporamide injection in *Fmr1*^{-/-} mice. Thus, cercosporamide blocks Mnk kinase activity and selectively inhibits *Mmp9* translation through reduced phosphorylation of eIF4E. These data are consistent with previous work demonstrating that lovastatin, a drug prescribed for treatment of high cholesterol, inhibits Ras-ERK1/2 upstream of phospho-eIF4E, corrects excessive protein synthesis, and prevents epileptogenesis in *Fmr1*^{-/-} mice (Osterweil et al., 2013).

eIF4E Phosphorylation and MMP-9 Overexpression as a Potential Therapeutic Target in FXS/ASD, Downstream of Group 1 mGluRs/ Ras/ERK/Mnk

Increased amounts of MMP-9 (Figure 2), but not deletion of *Mmp9* (Figure 6), engender FXS/ASD-like phenotypes. The lack of social deficits in *Mmp9*^{-/-} could be conceivably

explained by homeostatic regulation of other members of the MMP family. Mice overexpressing MMP-9 recapitulate several FXS-like phenotypes, indicating that Mmp-9 is responsible for a significant part of the *Fmr1*^{-y} phenotype (Figure 2), which is consistent with the increased translation of *Mmp9* mRNA observed in *Fmr1*^{-y} mice (Figure 1). In particular, deletion of *Mmp9* in *Fmr1*^{-y} mice, rescued synaptic, dendritic spine, and behavioral deficits, further supporting the notion that Mmp-9 is a master player in FXS phenotypes (Sidhu et al., 2014). Mmp-9 is a crucial target downstream of mGluRs/Mnk/phospho-eIF4E, because it remodels the extracellular matrix by proteolyzing some of its components, such as cell adhesion molecules, extracellular proteins, and potentially receptor subunits (Huntley, 2012). These activities of MMP-9 may intersect with those of proteins implicated in ASD/FXS that are important for synaptic function and maturation. Thus, restoring normal *Mmp9* translation impacts the regulation of several Mmp-9 targets, which are associated with FXS/ASD. Moreover, Mmp-9 is downstream of group 1 mGluRs, and it offers an appealing and selective avenue for treatment that would exclude off-target upstream effects.

EXPERIMENTAL PROCEDURES

Knockin and Knockout Mice

Eif4e^{ki} (knockin Ser209Ala) mice were previously described (Furic et al., 2010). *Fmr1*^{-y}, *Mmp9*^{-/-}, and *Mnk1*^{+/-}/*Mnk2*^{+/-} mice were on the C57Bl/6 background (Jackson Laboratories). All procedures were in compliance with the Canadian Council on Animal Care guidelines and were approved by McGill University, Université de Montréal, NCSR Demokritos Animal Care Committees and by the Eli Lilly and Company Institutional Animal Care and Use Committee.

Polysome Profile Analysis and qRT-PCR

Polysome profile analysis and qRT-PCR were carried out as described (Gkogkas et al., 2013).

Western Blotting and Antibodies

All tissues were dissociated in RIPA buffer (unless otherwise specified). Western blotting was previously described (Gkogkas et al., 2013).

Three-Chamber Social Approach and Preference for Social Novelty Tests

A three-chamber arena was used to assess social approach and preference for social novelty and was previously described (Gkogkas et al., 2013).

Self-Grooming Test

Mice were placed in a Plexiglas cage with fresh bedding and no nest or cardboard material. Self-grooming behavior was recorded for 10 min following an initial 10 min habituation phase.

Social Interaction with Juvenile Male or Female Tests

Experimental and stimulus mice (juvenile 4-week-old C57Bl/6 male or 12-week-old C57BL/6 female) were habituated to the experimental room and the Plexiglas cage for 5 min. The unfamiliar stimulus mouse was then introduced into the testing cage and left there for 5 min. Aggression, interaction and affiliation, and self-grooming were scored.

Light-Dark Transition Test

The test apparatus was composed of two chambers: a dark enclosed chamber composed of wood (15 × 21 × 21 cm) and a larger chamber (30 × 21 × 21 cm) with three clear Plexiglas walls and an open top. The two chambers are connected by a small opening. Mice were placed into the “light” side and allowed to explore freely for 10 min. An entry was defined as the mouse placing all 4 ft into each zone.

Open-Field Exploration

Mice were placed into the center of a 40 × 40 × 30 cm chamber. Data were collected in 2 min intervals for each mouse for 30 min. The number of entries into the center square, which was used as a measure of anxiety-like behavior was calculated.

Audiogenic Seizures

The test apparatus consisted of a Plexiglas cylinder (40 cm diameter and 60 cm deep) covered by a plate with a 120 dB alarm as described in Musumeci et al. (2007).

Analysis of Neuronal Morphology by Golgi-Cox Staining

Rapid GolgiKit (FD NeuroTechnologies) was used for the staining procedure according to the manufacturer's instructions as described in Gkogkas et al. (2013).

Electrophysiology

Electrophysiological experiments were performed as previously described (Khoutorsky et al., 2013) with some modifications.

Measurement of De Novo Protein Synthesis

Transverse hippocampal slices (400 μm) were prepared from 5- to 6-week-old mice and allowed to recover for at least 3 hr. Puromycin labeling was performed as described previously (Hoeffler et al., 2011; Bhattacharya et al., 2012) with some modifications.

Statistical Analysis

Experimenters were blinded to the genotype during testing and scoring. All data are presented as mean ± SEM (error bars). Statistical significance was set a priori at 0.05 (NS, nonsignificant). Details for tests used are provided in the figure legends and Supplemental Experimental Procedures.

Supplementary Material

Refer to Web version on PubMed Central for supplementary material.

ACKNOWLEDGMENTS

This work was supported by a CIHR operating grant to N.S. (MOP-114994) and J.-C.L. (MOP-125985), the Azrieli Foundation and Brain Canada team grant to N.S. and J.-C.L., the Fonds de la Recherche en Santé (grant to J.-C.L. FRQS; Groupe de Recherche sur le Système Nerveux Central). J.-C.L. is the recipient of the Canada Research Chair in Cellular and Molecular Neurophysiology. C.G.G. received support from the Wellcome Trust-University of Edinburgh Institutional Strategic Support Fund. Human tissue was obtained from the NICHD Brain and Tissue Bank for Developmental Disorders at the University of Maryland, Baltimore and the Harvard Brain Tissue Resource Center (grant number R24-MH 068855). We thank P. Hagerman and G. Espinal-Goyne for FXS postmortem brain samples and A. Sylvestre, S. Perreault, C. Lister, K. Gamache, and I. Harvey for technical assistance. J.R.G. and B.W.K. are employees of Eli Lilly and Company.

REFERENCES

- Abdallah MW, Pearce BD, Larsen N, Greaves-Lord K, Nørgaard-Pedersen B, Hougaard DM, Mortensen EL, Grove J. Amniotic fluid MMP-9 and neurotrophins in autism spectrum disorders: an exploratory study. *Autism Res.* 2012; 5:428–433. [PubMed: 23008271]
- Ascano M Jr, Mukherjee N, Bandaru P, Miller JB, Nusbaum JD, Corcoran DL, Langlois C, Munschauer M, Dewell S, Hafner M, et al. FMRP targets distinct mRNA sequence elements to regulate protein expression. *Nature.* 2012; 492:382–386. [PubMed: 23235829]
- Banko JL, Hou L, Klann E. NMDA receptor activation results in PKA- and ERK-dependent Mnk1 activation and increased eIF4E phosphorylation in hippocampal area CA1. *J. Neurochem.* 2004; 91:462–470. [PubMed: 15447679]
- Bear MF, Huber KM, Warren ST. The mGluR theory of fragile X mental retardation. *Trends Neurosci.* 2004; 27:370–377. [PubMed: 15219735]
- Bhattacharya A, Kaphzan H, Alvarez-Dieppa AC, Murphy JP, Pierre P, Klann E. Genetic removal of p70 S6 kinase 1 corrects molecular, synaptic, and behavioral phenotypes in fragile X syndrome mice. *Neuron.* 2012; 76:325–337. [PubMed: 23083736]
- Bilousova TV, Dansie L, Ngo M, Aye J, Charles JR, Ethell DW, Ethell IM. Minocycline promotes dendritic spine maturation and improves behavioural performance in the fragile X mouse model. *J. Med. Genet.* 2009; 46:94–102. [PubMed: 18835858]
- Bozdagi O, Nagy V, Kwei KT, Huntley GW. In vivo roles for matrix metalloproteinase-9 in mature hippocampal synaptic physiology and plasticity. *J. Neurophysiol.* 2007; 98:334–344. [PubMed: 17493927]
- Budimirovic DB, Kaufmann WE. What can we learn about autism from studying fragile X syndrome? *Dev. Neurosci.* 2011; 33:379–394. [PubMed: 21893949]
- Buxade M, Parra-Palau JL, Proud CG. The MnkS: MAP kinase-interacting kinases (MAP kinase signal-integrating kinases). *Front. Biosci.* 2008; 13:5359–5373. [PubMed: 18508592]
- Chen E, Sharma MR, Shi X, Agrawal RK, Joseph S. Fragile X mental retardation protein regulates translation by binding directly to the ribosome. *Mol. Cell.* 2014; 54:407–417. [PubMed: 24746697]
- Dansie LE, Phommahaxay K, Okusanya AG, Uwadia J, Huang M, Rot-schafer SE, Razak KA, Ethell DW, Ethell IM. Long-lasting effects of minocycline on behavior in young but not adult Fragile X mice. *Neuroscience.* 2013; 246:186–198. [PubMed: 23660195]
- Darnell JC, Van Driesche SJ, Zhang C, Hung KY, Mele A, Fraser CE, Stone EF, Chen C, Fak JJ, Chi SW, et al. FMRP stalls ribosomal translocation on mRNAs linked to synaptic function and autism. *Cell.* 2011; 146:247–261. [PubMed: 21784246]
- Dziembowska M, Pretto DI, Janusz A, Kaczmarek L, Leigh MJ, Gabriel N, Durbin-Johnson B, Hagerman RJ, Tassone F. High MMP-9 activity levels in fragile X syndrome are lowered by minocycline. *Am. J. Med. Genet. A.* 2013; 161A:1897–1903. [PubMed: 23824974]
- Elsabbagh M, Divan G, Koh YJ, Kim YS, Kauchali S, Marcín C, Montiel-Nava C, Patel V, Paula CS, Wang C, et al. Global prevalence of autism and other pervasive developmental disorders. *Autism Res.* 2012; 5:160–179. [PubMed: 22495912]

- Fragkouli A, Papatheodoropoulos C, Georgopoulos S, Stamatakis A, Stylianopoulou F, Tsilibary EC, Tzinia AK. Enhanced neuronal plasticity and elevated endogenous sAPPa levels in mice over-expressing MMP9. *J. Neurochem.* 2012; 121:239–251. [PubMed: 22192143]
- Furic L, Rong L, Larsson O, Koumakpayi IH, Yoshida K, Brueschke A, Petroulakis E, Robichaud N, Pollak M, Gaboury LA, et al. eIF4E phosphorylation promotes tumorigenesis and is associated with prostate cancer progression. *Proc. Natl. Acad. Sci. USA.* 2010; 107:14134–14139. [PubMed: 20679199]
- Gkogkas CG, Khoutorsky A, Ran I, Rampakakis E, Nevarko T, Weatherill DB, Vasuta C, Yee S, Truitt M, Dallaire P, et al. Autism-related deficits via dysregulated eIF4E-dependent translational control. *Nature.* 2013; 493:371–377. [PubMed: 23172145]
- Graber TE, Hébert-Seropian S, Khoutorsky A, David A, Yewdell JW, Lacaille JC, Sossin WS. Reactivation of stalled polyribosomes in synaptic plasticity. *Proc. Natl. Acad. Sci. USA.* 2013; 110:16205–16210. [PubMed: 24043809]
- Hagerman R, Hagerman P. Advances in clinical and molecular understanding of the FMR1 premutation and fragile X-associated tremor/ataxia syndrome. *Lancet Neurol.* 2013; 12:786–798. [PubMed: 23867198]
- Hay N, Sonenberg N. Upstream and downstream of mTOR. *Genes Dev.* 2004; 18:1926–1945. [PubMed: 15314020]
- Hoeffler CA, Cowansage KK, Arnold EC, Banko JL, Moerke NJ, Rodriguez R, Schmidt EK, Klosi E, Chorev M, Lloyd RE, et al. Inhibition of the interactions between eukaryotic initiation factors 4E and 4G impairs long-term associative memory consolidation but not reconsolidation. *Proc. Natl. Acad. Sci. USA.* 2011; 108:3383–3388. [PubMed: 21289279]
- Hoeffler CA, Sanchez E, Hagerman RJ, Mu Y, Nguyen DV, Wong H, Whelan AM, Zukin RS, Klann E, Tassone F. Altered mTOR signaling and enhanced CYFIP2 expression levels in subjects with fragile X syndrome. *Genes Brain Behav.* 2012; 11:332–341. [PubMed: 22268788]
- Huber KM, Roder JC, Bear MF. Chemical induction of mGluR5- and protein synthesis—dependent long-term depression in hippocampal area CA1. *J. Neurophysiol.* 2001; 86:321–325. [PubMed: 11431513]
- Huntley GW. Synaptic circuit remodelling by matrix metalloproteinases in health and disease. *Nat. Rev. Neurosci.* 2012; 13:743–757. [PubMed: 23047773]
- Janusz A, Milek J, Perycz M, Pacini L, Bagni C, Kaczmarek L, Dziembowska M. The Fragile X mental retardation protein regulates matrix metalloproteinase 9 mRNA at synapses. *J. Neurosci.* 2013; 33:18234–18241. [PubMed: 24227732]
- Kelleher RJ 3rd, Govindarajan A, Jung HY, Kang H, Tonegawa S. Translational control by MAPK signaling in long-term synaptic plasticity and memory. *Cell.* 2004; 116:467–479. [PubMed: 15016380]
- Khoutorsky A, Yanagiya A, Gkogkas CG, Fabian MR, Prager-Khoutorsky M, Cao R, Gamache K, Bouthiette F, Parsyan A, Sorge RE, et al. Control of synaptic plasticity and memory via suppression of poly(A)-binding protein. *Neuron.* 2013; 78:298–311. [PubMed: 23622065]
- Konicek BW, Stephens JR, McNulty AM, Robichaud N, Peery RB, Dumstorf CA, Dowless MS, Iversen PW, Parsons S, Ellis KE, et al. Therapeutic inhibition of MAP kinase interacting kinase blocks eukaryotic initiation factor 4E phosphorylation and suppresses outgrowth of experimental lung metastases. *Cancer Res.* 2011; 71:1849–1857. [PubMed: 21233335]
- Leigh MJ, Nguyen DV, Mu Y, Winarni TI, Schneider A, Chechi T, Polussa J, Doucet P, Tassone F, Rivera SM, et al. A randomized double-blind, placebo-controlled trial of minocycline in children and adolescents with fragile x syndrome. *J. Dev. Behav. Pediatr.* 2013; 34:147–155. [PubMed: 23572165]
- McKinney BC, Grossman AW, Elisseou NM, Greenough WT. Dendritic spine abnormalities in the occipital cortex of C57BL/6 Fmr1 knockout mice. *Am. J. Med. Genet. B. Neuropsychiatr. Genet.* 2005; 136B:98–102. [PubMed: 15892134]
- Musumeci SA, Calabrese G, Bonaccorso CM, D'Antoni S, Brouwer JR, Bakker CE, Elia M, Ferri R, Nelson DL, Oostra BA, Catania MV. Audiogenic seizure susceptibility is reduced in fragile X knockout mice after introduction of FMR1 transgenes. *Exp. Neurol.* 2007; 203:233–240. [PubMed: 17007840]

- Osterweil EK, Krueger DD, Reinhold K, Bear MF. Hypersensitivity to mGluR5 and ERK1/2 leads to excessive protein synthesis in the hippocampus of a mouse model of fragile X syndrome. *J. Neurosci.* 2010; 30:15616–15627. [PubMed: 21084617]
- Osterweil EK, Chuang SC, Chubykin AA, Sidorov M, Bianchi R, Wong RK, Bear MF. Lovastatin corrects excess protein synthesis and prevents epileptogenesis in a mouse model of fragile X syndrome. *Neuron.* 2013; 77:243–250. [PubMed: 23352161]
- Rotschafer SE, Trujillo MS, Dansie LE, Ethell IM, Razak KA. Minocycline treatment reverses ultrasonic vocalization production deficit in a mouse model of Fragile X Syndrome. *Brain Res.* 2012; 1439:7–14. [PubMed: 22265702]
- Rudelli RD, Brown WT, Wisniewski K, Jenkins EC, Laure-Kamionowska M, Connell F, Wisniewski HM. Adult fragile X syndrome. Clinico-neuropathologic findings. *Acta Neuropathol.* 1985; 67:289–295. [PubMed: 4050344]
- Santini E, Huynh TN, MacAskill AF, Carter AG, Pierre P, Ruggiero D, Kaphzan H, Klann E. Exaggerated translation causes synaptic and behavioural aberrations associated with autism. *Nature.* 2013; 493:411–415. [PubMed: 23263185]
- Schmidt EK, Clavarino G, Ceppi M, Pierre P. SUNSET, a nonradioactive method to monitor protein synthesis. *Nat. Methods.* 2009; 6:275–277. [PubMed: 19305406]
- Seyfried TN, Yu RK, Glaser GH. Genetic analysis of audiogenic seizure susceptibility in C57BL/6J X DBA/2J recombinant inbred strains of mice. *Genetics.* 1980; 94:701–718. [PubMed: 7399258]
- Sharma A, Hoeffler CA, Takayasu Y, Miyawaki T, McBride SM, Klann E, Zukin RS. Dysregulation of mTOR signaling in fragile X syndrome. *J. Neurosci.* 2010; 30:694–702. [PubMed: 20071534]
- Sidhu H, Dansie LE, Hickmott PW, Ethell DW, Ethell IM. Genetic removal of matrix metalloproteinase 9 rescues the symptoms of fragile X syndrome in a mouse model. *J. Neurosci.* 2014; 34:9867–9879. [PubMed: 25057190]
- Silverman JL, Yang M, Lord C, Crawley JN. Behavioural phenotyping assays for mouse models of autism. *Nat. Rev. Neurosci.* 2010; 11:490–502. [PubMed: 20559336]
- Spencer CM, Alekseyenko O, Serysheva E, Yuva-Paylor LA, Paylor R. Altered anxiety-related and social behaviors in the Fmr1 knockout mouse model of fragile X syndrome. *Genes Brain Behav.* 2005; 4:420–430. [PubMed: 16176388]
- Sutherland GR, Ashforth PL. X-linked mental retardation with macro-orchidism and the fragile site at Xq 27 or 28. *Hum. Genet.* 1979; 48:117–120. [PubMed: 572332]
- The Dutch-Belgian Fragile X Consortium. Fmr1 knockout mice: a model to study fragile X mental retardation. *Cell.* 1994; 78:23–33. [PubMed: 8033209]
- Udagawa T, Farny NG, Jakovcevski M, Kaphzan H, Alarcon JM, Anil-kumar S, Ivshina M, Hurt JA, Nagaoka K, Nalavadi VC, et al. Genetic and acute CPEB1 depletion ameliorate fragile X pathophysiology. *Nat. Med.* 2013; 19:1473–1477. [PubMed: 24141422]
- Verkerk AJ, Pieretti M, Sutcliffe JS, Fu YH, Kuhl DP, Pizzuti A, Reiner O, Richards S, Victoria MF, Zhang FP, et al. Identification of a gene (FMR-1) containing a CGG repeat coincident with a breakpoint cluster region exhibiting length variation in fragile X syndrome. *Cell.* 1991; 65:905–914. [PubMed: 1710175]
- Wang X, Snape M, Klann E, Stone JG, Singh A, Petersen RB, Castellani RJ, Casadesus G, Smith MA, Zhu X. Activation of the extracellular signal-regulated kinase pathway contributes to the behavioral deficit of fragile x-syndrome. *J. Neurochem.* 2012; 121:672–679. [PubMed: 22393900]
- Waskiewicz AJ, Flynn A, Proud CG, Cooper JA. Mitogen-activated protein kinases activate the serine/threonine kinases Mnk1 and Mnk2. *EMBO J.* 1997; 16:1909–1920. [PubMed: 9155017]

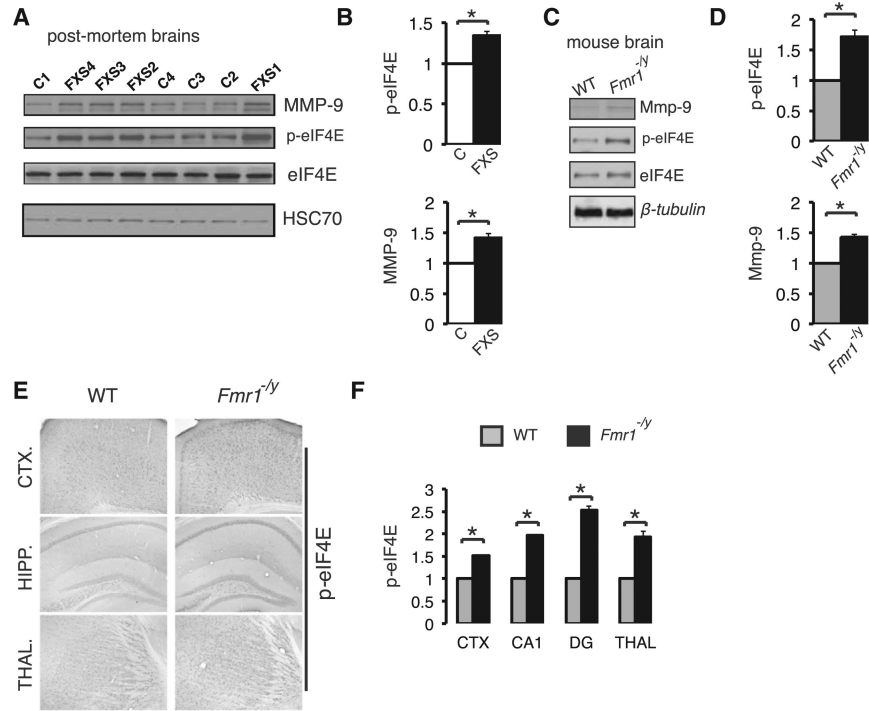


Figure 1. Elevated Phosphorylation of eIF4E and Increased Expression of MMP-9 in Postmortem Brains from FXS Patients and in *Fmr1*^{-/-} Mouse Brain

(A) Western blot analysis of lysates from frontal cortex or hippocampus from control “C” (n = 9) and FXS patients “FXS” (n = 8; see Figure S2). Representative images of immunoblots probed with antibodies against the indicated proteins are shown. HSC70 was the loading control.

(B) Quantification of western blots from (A). Protein amounts of phospho-eIF4E and MMP9 are normalized to total eIF4E and HSC70 (n = 3 for each group) and presented as fold change relative to control.

(C) Western blot analysis of whole-brain lysates from *Fmr1*^{-/-} and wild-type (WT) littermates (n = 3 for each group). Representative images of immunoblots probed with antibodies against the indicated proteins are shown; β -tubulin was the loading control.

(D) Quantification of data in (C) for phospho-eIF4E and Mmp9 protein amounts (n = 3 for each group), normalized to eIF4E and β -tubulin, respectively, and presented as fold change relative to WT.

(E) Immunohistochemical DAB staining of cortical (CTX.), hippocampal (HIPP.), and thalamic (THAL.) 50 μ m slices from WT and *Fmr1*^{-/-} mice. Representative images of slices stained with antibodies against the indicated proteins are shown.

(F) Quantification of immunohistochemical staining in (E) for phospho-eIF4E (n = 3 for each group; fold change relative to WT). For (A)–(F), Student's t test, *p < 0.05. See also Figure S2.

Data are presented as mean \pm SEM (error bars).

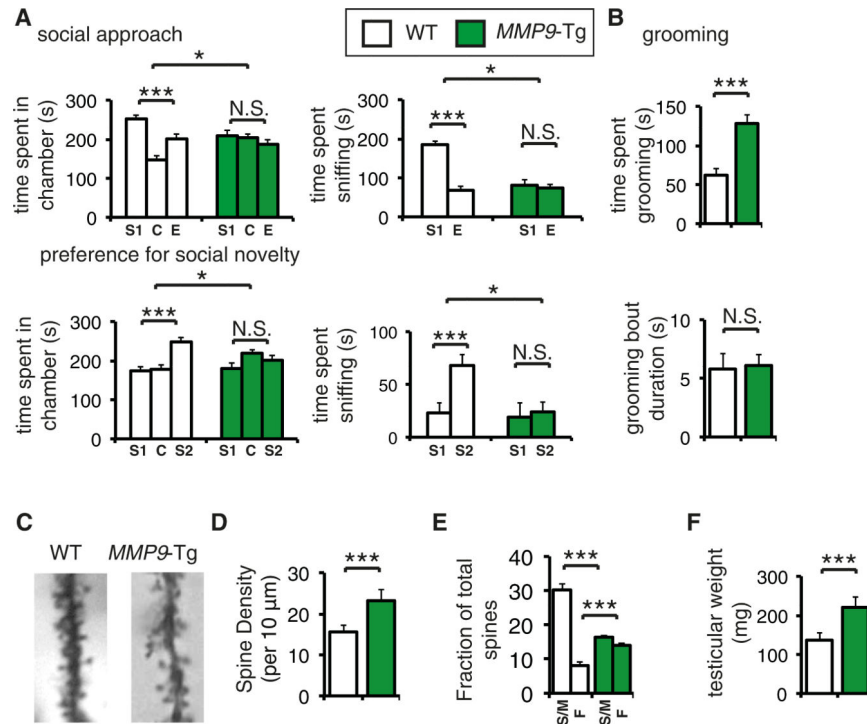


Figure 2. *MMP9*-Tg-Overexpressing Mice Display Autism/FXS-like Phenotypes

(A) Three-chamber social interaction test, showing time spent in each chamber (top left) and time spent sniffing each wire cage (top right); S1, stranger 1 (social stimulus); C, center compartment; E, empty wire-cage compartment (nonsocial stimulus). Preference for social novelty three-chamber social interaction test, showing time spent in each chamber (bottom left) and time spent interacting with the novel social stimulus (bottom right; stranger 2; S2) or the previously encountered mouse (stranger 1; S1); C, center compartment. $n = 14$ for each group; *** $p < 0.001$, * $p < 0.05$, twoway ANOVA with Bonferroni's post hoc.

(B) Self-grooming test, where the total time spent grooming is depicted; $n = 14$ per group

(C) Golgi-Cox staining of hippocampal CA1 dendritic spines from WT and *MMP9*-Tg mice. Representative images are shown.

(D) Quantification of spine density (spines per 10 μm) from images in (C).

(E) Spine subtype analysis (S/M, spiny/mushroom; F, filopodial) presented as a fraction of total spines for each subtype. *** $p < 0.001$, two-way ANOVA with Bonferroni's post hoc.

(F) Mean testicular weight (mg) of WT and *MMP9*-Tg P90-100 mice; $n = 12$ per group, *** $p < 0.001$; Student's *t* test. WT, wild-type; *MMP9*-Tg, litter-mates overexpressing *MMP9*.

Data are presented as mean \pm SEM (error bars). For (B) and (D), $n = 5$ per group, *** $p < 0.001$, Student's *t* test.

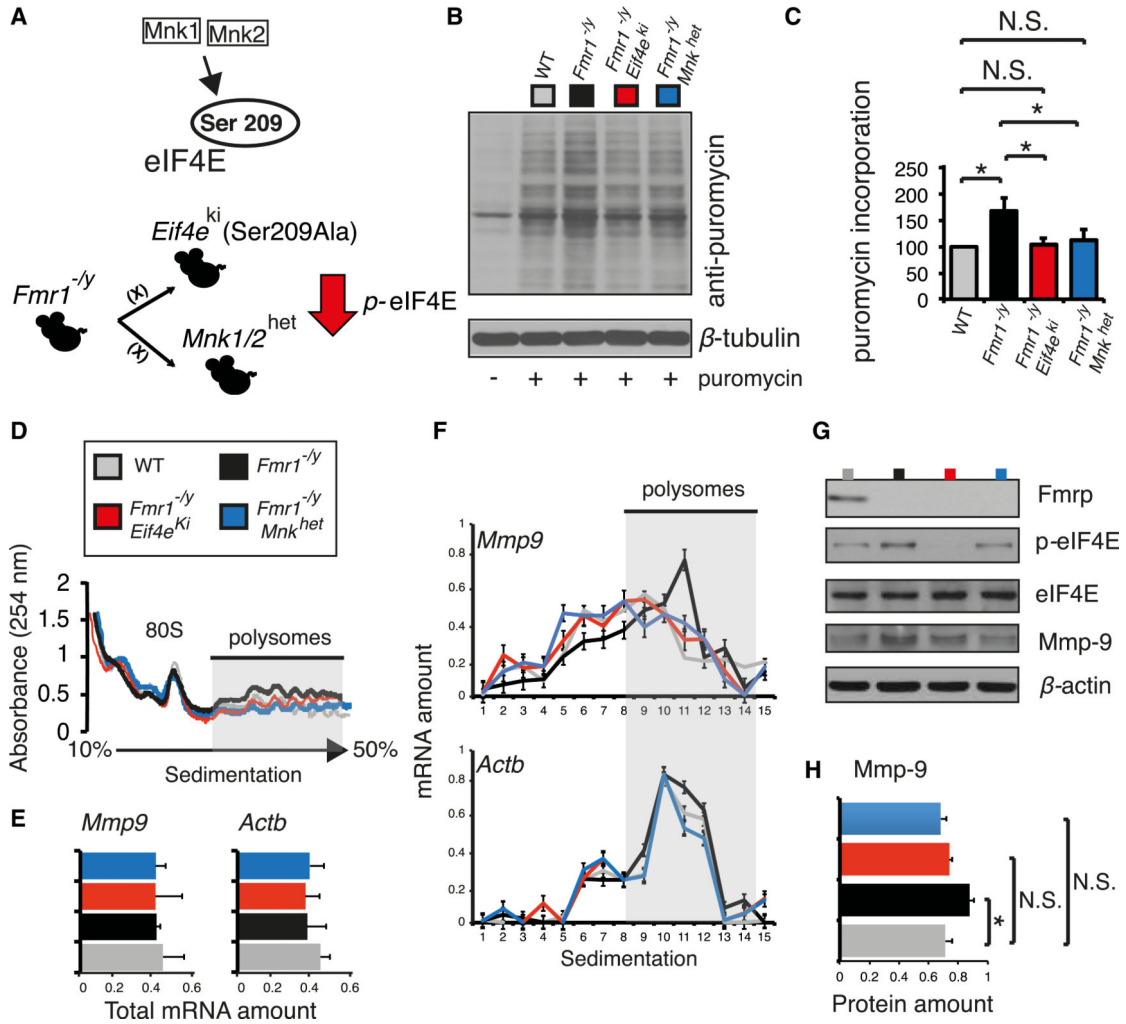


Figure 3. Phospho-eIF4E-Dependent Translation of *Mmp9* in FXS Model Mice

(A) Breeding scheme to acquire “double-mutant” mice, where eIF4E phosphorylation is depleted (*Fmr1*^{-/-}/*Eif4e*^{ki}) or significantly reduced (*Fmr1*^{-/-}/*Mnk*^{het}).

(B) Puromycin incorporation assay in the four genotypes examined: WT, *Fmr1*^{-/-}, *Fmr1*^{-/-}/*Eif4e*^{ki}, and *Fmr1*^{-/-}/*Mnk*^{het}. Puromycin-labeled CA1 hippocampal slices were lysed and subjected to immunoblotting; representative images of immunoblots are shown, probed with antibodies against the indicated proteins; β -tubulin was the loading control.

(C) Quantification of the puromycin incorporation assay in (B). Puromycin incorporation (puromycin antibody signal intensity) was normalized to the loading control and presented as percentage change relative to WT; n = 3, *p < 0.05, Student's t test.

(D) Polysome profiling in hippocampal lysates from the four indicated genotypes. Positions of the 80S ribosome peak and polysomes are indicated.

(E) Total mRNA amounts for *Mmp9* and *Actb* assessed by qRT-PCR in the four indicated genotypes.

(F) qRT-PCR on RNA extracted from polysome fractions. Distribution of indicated mRNAs is illustrated as relative mRNA amounts for the different fractions and normalized between different fractions to control; n = 4, Student's t test.

(G) Representative immunoblots from hippocampal lysates for the four indicated genotypes, probed with antibodies against the indicated proteins; β -actin was the loading control.

(H) Quantification of immunoblots from (G); $n = 4$, Mmp-9 protein amounts are normalized to β -actin. * $p < 0.05$ Student's t test. See also Figure S3. Data are presented as mean \pm SEM (error bars).

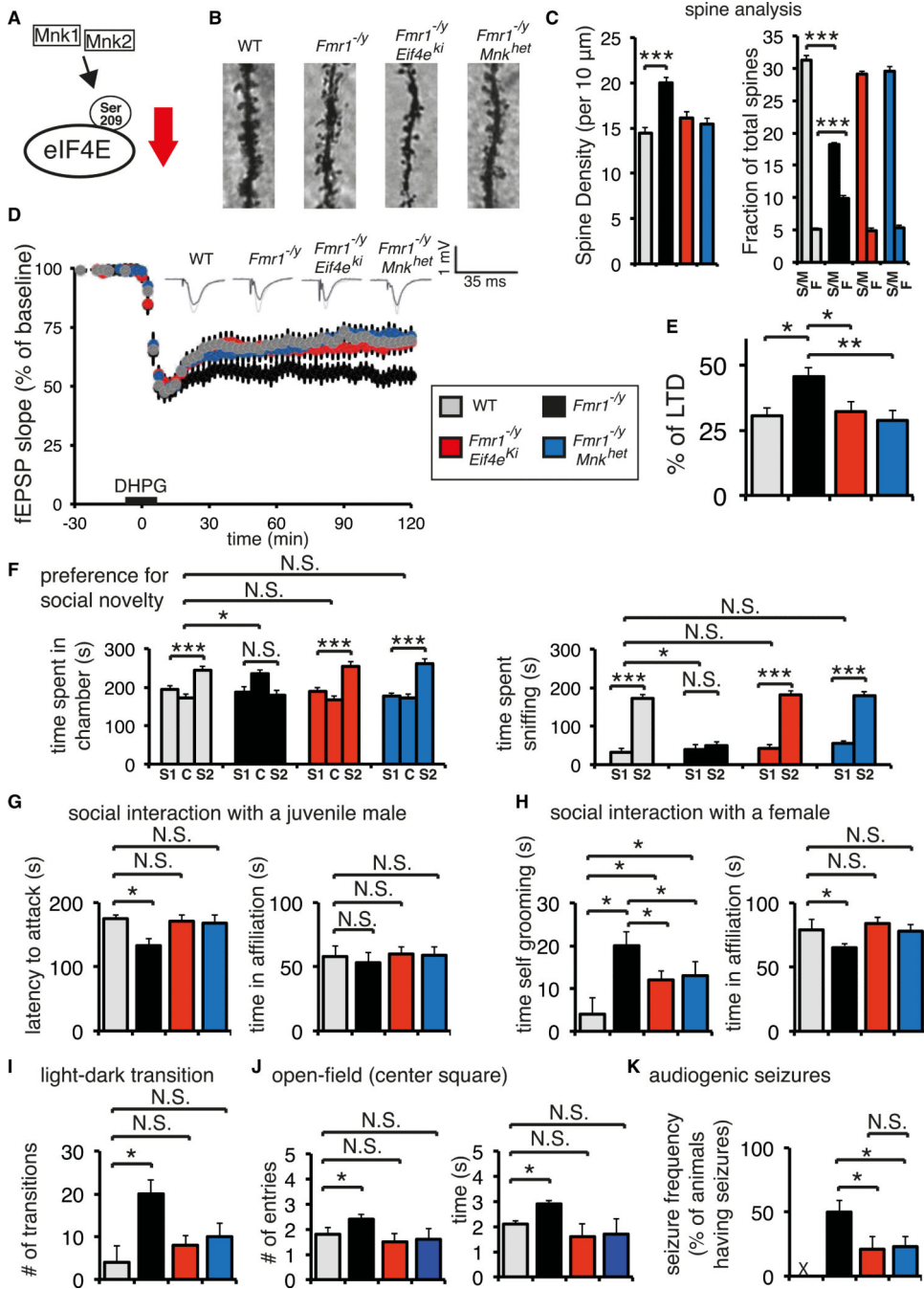


Figure 4. Genetic Reduction of eIF4E Phosphorylation Rescues FXS-like Phenotypes

(A) Haploinsufficiency of *Mnk1* and *Mnk2* or alanine mutation of Ser209 in eIF4E inhibits eIF4E phosphorylation in mice.

(B) Golgi-Cox staining of CA1 dendritic spines in four genotypes: WT, *Fmr1*^{-/-}, *Fmr1*^{-/-} *Eif4e*^{Ki}, and *Fmr1*^{-/-} *Mnk*^{het}.

(C) Quantification of spine analysis for (B). Spine density for the four indicated phenotypes is measured as the number of spines per 10 μm; n = 5 per group, ***p < 0.001, Student's t test. Spine subtype analysis (S/M, spiny/mushroom; F, filopodial), presented as a fraction of

total spines for each subtype; $n = 5$ per group, $***p < 0.001$, two-way ANOVA with Bonferroni's post hoc.

(D) mGluR-LTD was induced with DHPG ($50 \mu\text{M}$ for 10 min) in hippocampal slices prepared from mice of the four indicated genotypes.

(E) Summary bar graph showing mGluR-LTD at 110–120 min period postinduction. Scale bar, 5 ms and 1 mV. $*p < 0.05$, $**p < 0.01$, one-way ANOVA with Bonferroni's post hoc. ($n = \text{WT}$ [14], *Fmr1*^{-/-} [25], *Fmr1*^{-/-}/*Eif4e*^{ki} [16], *Fmr1*^{-/-}/*Mnk*^{het} [16].) See also Figure S4B.

(F) Preference for social novelty three-chamber social interaction test, showing time spent in each chamber (LEFT) and time spent interacting with the novel social stimulus (right; stranger 2; S2) or the previously encountered mouse (stranger 1; S1); C, center compartment.

(G) Social interaction with a juvenile male mouse test. Latency to attack and time spent in affiliation are measured for the indicated genotypes.

(H) Social interaction with a female mouse test. Time engaged in self-grooming and time spent in affiliation are measured for the indicated genotypes.

(I) Light-dark transition test. Number of transitions between the light and dark compartments is depicted for the indicated genotypes.

(J) Open-field exploration. Number of entries and time spent in the center square of an open field is measured for the four genotypes.

(K) Audiogenic seizure frequency (percentage of animals having seizures) for the indicated genotypes. X marks resistance of WT mice to AGS.

For (F)–(K), $n = 14$ for each group; $***p < 0.001$, $*p < 0.05$, two-way ANOVA with Bonferroni's post hoc. See also Figure S4. Data are presented as mean \pm SEM (error bars).

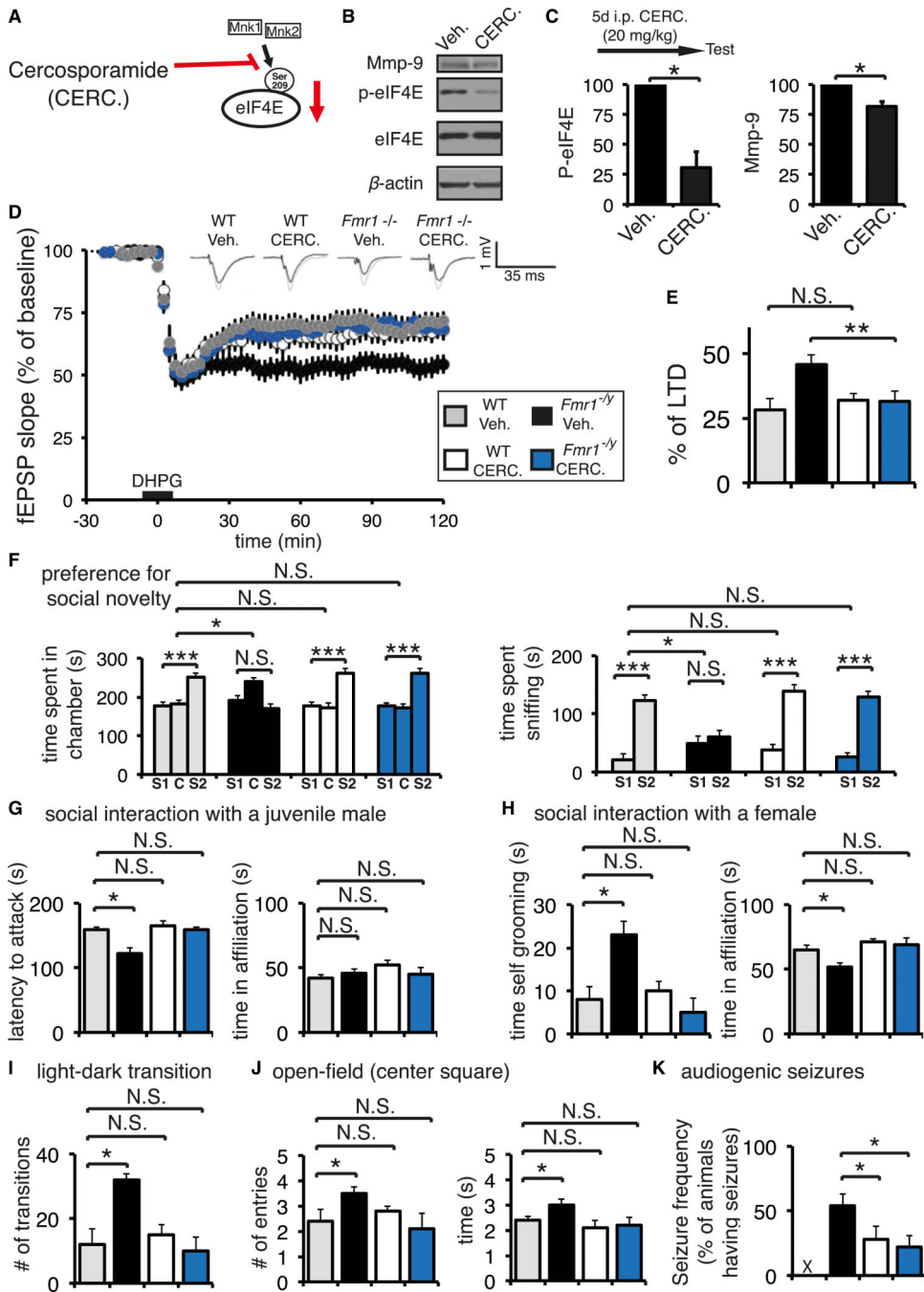


Figure 5. Pharmacological Inhibition of eIF4E Phosphorylation Rescues FXS-like Phenotypes

(A) Cercosporamide (CERC.) is a selective potent inhibitor of Mnk1/Mnk2 and thus of phospho-eIF4E.

(B) Western blot of hippocampal lysates from WT and *Fmr1*^{-/-} mice injected with vehicle or treated chronically with cercosporamide (20 mg/kg). Representative immunoblots are shown, probed with antibodies against the indicated proteins; β -actin was the loading control.

(C) Quantification of western blots from (B); $n = 3$, phospho-eIF4E protein amounts are normalized to eIF4E and presented as percentage change relative to vehicle. $*p < 0.05$ Student's t test.

(D and E) *Fmr1*^{-/-} (Veh., $n = 18$; Cerc., $n = 17$) and WT (Veh., $n = 14$; Cerc., $n = 10$) mice were injected daily with cercosporamide (20 mg/kg) or vehicle for 5 consecutive days and 1 hr after the last injection hippocampal slices were prepared. Enhanced mGluR-LTD in *Fmr1*^{-/-} slices was normalized after chronic treatment with cercosporamide. Scale bar, 5 ms and 1 mV; $**p < 0.03$, using one-way ANOVA followed by Bonferroni post hoc tests.

(F) Preference for social novelty three-chamber social interaction test, showing time spent in each chamber (LEFT) and time spent interacting with the novel social stimulus (right; stranger 2; S2) or the previously encountered mouse (stranger 1; S1); C, center compartment.

(G) Social interaction with a juvenile male mouse test. Latency to attack and time spent in affiliation are measured for the indicated genotypes.

(H) Social interaction with a female mouse test. Time engaged in self-grooming and time spent in affiliation are depicted.

(I) Light-dark transition test. Number of transitions between the light and dark compartments is shown.

(J) Open-field exploration. Number of entries and time spent in the center square of an open field is measured.

(K) Audiogenic seizure frequency (% of animals having seizures). X marks resistance of WT mice to AGS.

For (F)–(K), $n = 12$ for each group; $***p < 0.001$, $*p < 0.05$, two-way ANOVA with Bonferroni's post hoc. See also Figures S5 and 6. Data are presented as mean \pm SEM (error bars).

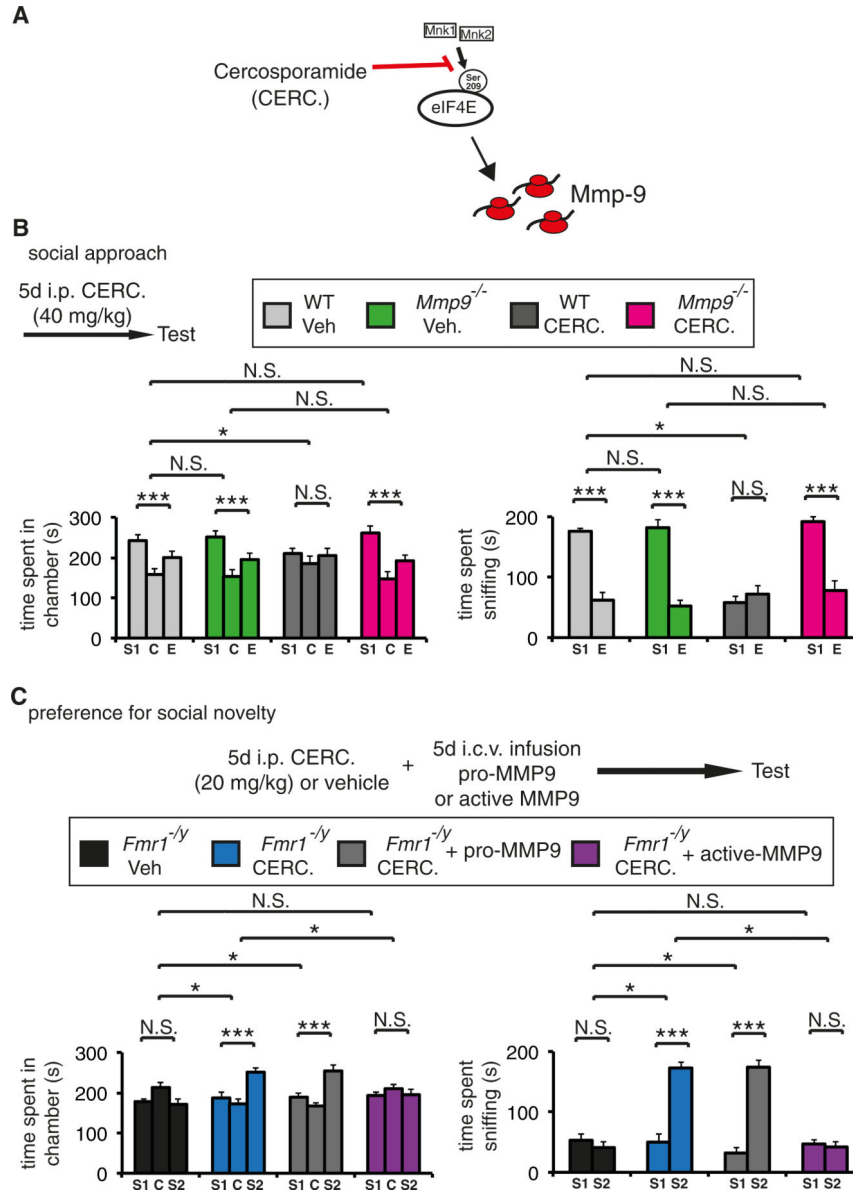


Figure 6. *Mmp9* Is a Critical Target of Phospho-eIF4E-Dependent Translation in *Fmr1*^{-/-} Mice (A) *Mmp9* is translationally controlled by phospho-eIF4E in FXS.

(B) Three-chamber social interaction test in WT or *Mmp9*^{-/-} mice, injected with vehicle or a chronic (5 days), “above-threshold” dose of cercospor-amide (CERC.; 40 mg/kg). Time spent in each chamber (left) and time spent sniffing each wire cage (right), are shown; S1, stranger 1 (social stimulus); C, center compartment; E, empty wire-cage compartment (nonsocial stimulus).

(C) Preference for social novelty three-chamber social interaction test in WT and *Fmr1*^{-/-} vehicle or cercosporamide (20 mg/kg, 5 days) treated, and simultaneously infused with recombinant pro or active forms of *Mmp9* (0.1 µg/µl, 2 µl per dose, two times a day for 5 days). Time spent in each chamber (LEFT) and time spent interacting with the novel social stimulus (right; stranger 2; S2) or the previously encountered mouse (stranger 1; S1); C,

center compartment; i.c.v., intracerebroventricular infusion. For (B) and (C), n = 10 for each group; ***p < 0.001, *p < 0.05, two-way ANOVA with Bonferroni's post hoc. Data are presented as mean \pm SEM (error bars).